Research Square

Preprints are preliminary reports that have not undergone peer review.
They should not be considered conclusive, used to inform clinical practice,
or referenced by the media as validated information.

Drivers of Wave Attenuation by Mangroves across contrasting geomorphic settings in Colombia

Maria Fernanda Acosta-Silva

macostas@unal.edu.co

Universidad Nacional de Colombia https://orcid.org/0009-0004-7613-6526

David Alejandro Sánchez-Núñez

Universidad Nacional de Colombia

Cesar David Padilla Mendoza

Universidad Nacional de Colombia

Jose Ernesto Mancera-Pineda

Universidad Nacional de Colombia

Research Article

Keywords: Coastal protection, Nature-based Solutions, Geomorphic settings, Rhizophora mangle

Posted Date: September 22nd, 2026

DOI: https://doi.org/10.21203/rs.3.rs-10855742/v1

License: This work is licensed under a Creative Commons Attribution 4.0 International License.
Read Full License

Drivers of Wave Attenuation by Mangroves across contrasting geomorphic settings in Colombia

Shipping date: 28/08/2026

Maria Fernanda Acosta-Silva [1], David Alejandro Sánchez-Núñez [2*], Cesar Padilla Mendoza [3], Jose Ernesto Mancera-Pineda [4]

[1] Universidad Nacional de Colombia, sede La Paz. Dirección académica. La Paz, Colombia. macostas@unal.edu.co. ORCID 0009-0004-7613-6526

[2] Universidad Nacional de Colombia, sede La Paz. Dirección académica. La Paz, Colombia. dasanchezn@unal.edu.co. ORCID 0000-0002-9071-2962

[3] Universidad Nacional de Colombia, sede La Paz. Dirección académica. La Paz, Colombia. cpadillam@unal.edu.co. ORCID 0000-0002-1777-9730

[4] Universidad Nacional de Colombia, sede Bogotá. Bogotá, Colombia. jemancerap@unal.edu.co. ORCID 0000-0003-2948-3387

* Corresponding author:
David Alejandro Sánchez Núñez
ORCID: https://orcid.org/0000-0002-9071-2962
Email: dasanchezn@unal.edu.co

Summary

Mangroves provide vital coastal protection, yet their wave attenuation capacity is strongly modulated by forest structure and hydrodynamics—factors that typically vary across coastal geomorphic settings. However, empirical comparisons of wave attenuation rates among contrasting geomorphic settings remain scarce. We evaluated how morphometric and oceanographic regulators influence wave attenuation rates across varied geomorphic settings in Colombia, grouping six study areas into deltaic-lagoonal systems, lagoons, open coasts, and estuaries. Wave data were processed using Python-based routines, and attenuation was isolated by subtracting shoaling and breaking effects modeled in XBeach (Surfbeat mode). Volumetric density, wave height and tide height collectively explained most attenuation variability (adjusted $R^2 = 0.76$, $p = 0.004$), with the former two showing high local variability within settings and sites. Notably, an epiphyte-bearing site in Ciénaga Grande de Santa Marta exhibited a global record volumetric density (V_d = 0.014) and wave attenuation rate (r = 0.49 m^{-1}). While epiphytes significantly increased volumetric density (*Mann-Whitney U*, p = 0.024) and showed notable

attenuation gains, differences were not statistically significant (*Mann-Whitney U*, $p = 0.497$). Attenuation peaked in deltaic-lagoonal settings and was lowest in estuaries, though these differences lacked statistical significance. High local variability in incident wave height and root density (averaging 36% and 68% CV), alongside multifactorial regulation, likely masked broader regional trends driven by tidal regimes or epiphytes. Overall, wave attenuation is governed by complex interactions between volumetric density and hydrodynamic conditions, where local-scale variability can equal or exceed variability across geomorphic settings.

Key words

Coastal protection, Nature-based Solutions, Geomorphic settings, *Rhizophora mangle*

1. Introduction

Coastal erosion driven by sea-level rise, wave action, and extreme meteorological events poses a major threat to tropical and subtropical shorelines worldwide (Banco Mundial, 2024). These processes compromise coastal infrastructure, alter sediment dynamics, and reduce the resilience of socio-ecological systems (Simpson et al., 2010). In response, Nature-based Solutions (NbS) have gained attention as sustainable alternatives for coastal protection, particularly where conventional engineering is economically or environmentally constrained (Narayan et al., 2016; Van Zelst et al., 2021). Mangrove forests are among the most effective ecosystems for wave attenuation and shoreline stabilization, reducing erosion rates three- to fifteen-fold relative to adjacent unvegetated environments (Sánchez-Núñez et al., 2019).

At broad spatial scales, geomorphic settings and wave exposure are expected to regulate wave attenuation. Mangroves develop across diverse coastal environments—including deltaic systems, estuaries, lagoons, and reef-protected shorelines—each characterized by distinct hydrodynamic regimes and sedimentary processes (Woodroffe, 1992; Alongi, 2009). However, previous empirical studies on wave attenuation have focused predominantly on single geomorphic settings (e.g., Zhang et al., 2022). Most research originates from Southeast Asia and relies on isolated local-scale observations, limiting our understanding of how regional tidal regimes, geomorphic settings, and vegetation structure interact under contrasting tropical conditions (Horstman et al., 2014; Mullarney et al., 2017).

This knowledge gap is particularly critical in Latin America, where empirical data across spatial scales remains scarce. In Colombia, the Caribbean and Pacific coasts exhibit fundamentally different oceanographic regimes and geomorphic settings. The Caribbean coast is microtidal and characterized by relatively low wave energy, facilitating the development of open-coast and lagoonal systems, as well as deltaic-lagoonal complexes where major rivers discharge. On the Pacific coast, high mesotidal regimes promote estuarine geomorphic settings (INVEMAR, 2022; Worthington et al., 2020). Furthermore, mangroves along the Colombian Caribbean develop across a wide diversity of climates and landforms, including beaches, promontories, and deltaic spits (Bernal, 1996; Sánchez-Núñez et al., 2019; Vanegas et al., 2019; Blanco-Libreros et al., 2022). Even within a single geomorphic setting, differences in landforms, bathymetry, shoreline

orientation, and wave exposure can generate substantial spatial variability in attenuation rates (Horstman et al., 2014). To our knowledge, this is one of the first studies to systematically compare wave attenuation rates across four distinct geomorphic settings and contrasting wave exposition conditions (exposed, protected) using a standardized approach.

Wave attenuation results from complex eco-hydrodynamic interactions between incident waves and vegetation structure. Aboveground root systems increase hydraulic roughness, generate drag forces, and dissipate wave energy (Mazda et al., 1997; Massel et al., 1999). Greater root density consistently enhances hydraulic resistance (Quartel et al., 2007; Bao, 2011), while additional features, such as epiphytes colonizing prop roots in protected lagoons, further influence dissipation mechanisms (Sánchez-Núñez et al., 2020). Nevertheless, wave attenuation cannot be explained solely by vegetation structure. Wave transformation processes (shoaling, breaking, and bottom friction) and local hydrodynamic variables—such as tidal range, incident wave height, and water depth—strongly modulate how waves interact with submerged roots (Méndez & Losada, 2004; Nepf, 2012; Samiksha et al., 2019).

In this context, this study evaluates the influence of vegetation morphometry, bathymetric elevation changes, coastal geomorphology, and local oceanographic conditions on wave attenuation rates across multiple geomorphic settings, landforms, and exposures. We hypothesized that wave attenuation rates are jointly controlled by vegetation volumetric density and hydrodynamic context, with tidal range modulating drag efficiency. We further expected estuarine mangroves to exhibit lower attenuation rates than other settings, as higher mesotidal inundation limits wave interactions with the denser submerged root structures near the bed (Horstman et al., 2014; Wei et al., 2025).

2. Methodology

2.1 Study areas

Primary field data were obtained from four localities in Colombia: Ciénaga Grande de Santa Marta (CGSM), Alta Guajira, San Andrés Islands (SAI), and two sites within Buenaventura, hereafter referred to as Site A and Site B. In addition, processed data from three further localities — the Sinú River delta (Bahía de Cispatá and Punta Mestizos) and Islas del Rosario Archipelago (Isla Grande) — were obtained from the scientific literature (Sánchez-Núñez et al., 2020; Vanegas et

al., 2019). In total, seven localities across Colombia were analyzed, all dominated by Rhizophora mangle forests, detailed in Table 1. Each study site was classified according to its geomorphic setting and the local geomorphic landform. The macroscale geomorphic setting of each study site was classified following the global biophysical typology proposed by Worthington et al. (2020), which categorizes mangrove systems according to their dominant geomorphic and sedimentary environments. For systems composed of active deltas, relict deltaic deposits and interconnected coastal lagoons, the composite deltaic–lagoonal setting described by Woodroffe (1992) was adopted. Within each geomorphic setting, multiple mesoscale landforms and different degrees of wave exposure may occur (Sánchez-Núñez et al., 2019). The mesoscale landform occupied by each mangrove stand was identified based on the available geomorphological literature for each study site (Table 1). This hierarchical classification enabled comparisons among study sites at the macroscale (geomorphic setting) while accounting for local geomorphic controls on wave attenuation through the characterization of mesoscale landforms. Wave exposure was classified as protected when coastal geomorphology and bathymetry (such as coastal lagoons) and coral reefs strongly transform and dissipate waves before they reach mangroves. Conversely, exposed sites face less transformed, and therefore much stronger waves.

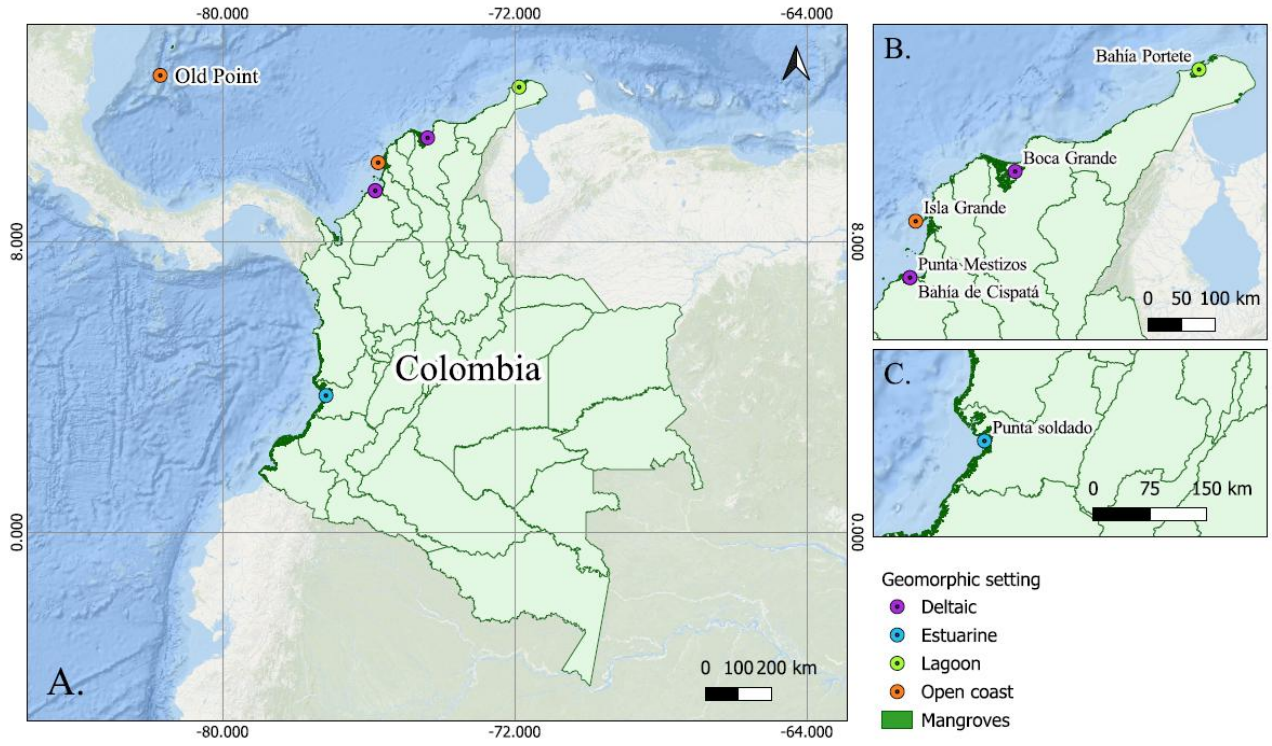
Table 1. Geographic location of wave attenuation data of this study. The geomorphic setting was classified according to terrigenous (T) and carbonate (C) sedimentary environments.

Study area	Locality (acronyms)	Macroscale geomorphic setting (sedimentary environment)	Mesoscale landform in which mangrove is located	Landform description	Wave exposure	Reference
Delta del río Sinú	Bahía de Cispatá (BC)	Deltaic-lagoonal (T)	Coastal lagoon	Lagoon system associated to a former delta of the Sinú River (Ruiz-Ochoa et al., 2008). Bahía de Cispatá comprises a lagoon complex covering approximately 16,000 ha, of which about 9000 ha correspond to water bodies and 7000 ha to mangrove forest.	Protected	Sánchez - Núñez et al., 2020

				The bay itself covers approximately 30 km^2 and has an average depth of 6 m (Bustos - Montes et al., 2012)		
Delta del río Sinú	Punta Mestizos (PM_1, PM_2)	Deltaic-lagoonal (T)	Deltaic spit	Deltaic spit formed within an abandoned deltaic lobe that was active from 1762 to 1849 (Piccardi et al., 2020). Owing to the loss of a sandbar around 1998, caused by a reduction in sediment yield from the Sinú River and wave erosion, mangroves are directly exposed to waves (Sánchez-Núñez et al., 2019)	Exposed	Sánchez - Núñez et al., 2020
Archipelago de Islas del Rosario	Isla Grande (IG)	Open coast (C)	Sandy beach	Mangroves patches are located in front of a sandy beach within a coral reef-lagoon complex (Cendales et al., 2002; Vanegas et al., 2019).	Protected	Vanegas et al., 2019
San Andrés Islas	Old Point Mangrove Regional Park (OP)	Open coast (C)	Promontory	A subtidal and intertidal fringe mangrove has developed along the front of the promontory within a coral reef-lagoon complex. Pleistocene coralline terraces, which overlie mangrove peat at this site and are colonized by dry forest, form the promontory that divides the two bays (Geister, 1973; Gamboa et al., 2012) and concentrates wave energy. Due to a gap in the coral reef barrier south of the island, this mangrove front experiences erosion during periods when	Protected	Present Study

				southern waves are strong (Echeverry et al., 2025)		
Ciénaga Grande de Santa Marta	Boca Grande (BG_1, BG_2)	Deltaic-lagoonal (T)	Coastal lagoon	Lagoonal mangrove system located within the CGSM delta-lagoon complex. It was formed by the reconfiguration of ancient fluvial deposits from a paleo-delta into a protected lagoonal environment (Bernal, 1996; Perdomo-Trujillo et al., 2021). The lagoon covers 450 km^2, creating a substantial fetch that allows the generation of local, wind waves	Protected	Present Study
Alta Guajira	Bahía Portete (BP)	Lagoon (T)	Coastal lagoon	A semi-enclosed shallow coastal system with restricted circulation (Kjerfve, 1994). Bahía Portete has an approximate water surface area of 125 km^2. A narrow inlet of approximately 2 km connects the lagoon with the Caribbean Sea (Gutierrez-Moreno et al., 2008)	Protected	Present Study
Buenaventura	Punta Soldado (PS_A_1, PS_A_2, PS_B)	Estuarine (T)	Barrier island sand flat	At the western side of the island, mangroves are located on a sand flat. At high tide, these mangroves face direct waves from the Pacific Ocean, which damage and kill trees at the mangrove edge (Niño y Eisinger, 2025). Punta soldado is a recessive barrier island that experience erosion rates up to 10.7 m $year^{-1}$ (Martínez et al., 2000)	Exposed	Present Study

Boca Grande in the Ciénaga Grande de Santa Marta is a deltaic-lagoonal complex located in the department of Magdalena, northern Colombia. This ecosystem is an important habitat for a wide diversity of species, and the mangrove forest is the most important vegetal coverage in this complex (Bernal, 1996; Rodríguez-Rodríguez et al, 2018). Similarly, Bahía de Cispatá and Punta Mestizos corresponds to a deltaic - lagoonal environment influenced by the discharge of the Sinú River and its interaction with the Caribbean Sea, defining its lagoonal configuration and hydrological connectivity (Ruiz-Ochoa et al., 2008). In contrast, Bahía Portete in La Guajira corresponds to a semi-arid coastal lagoon system, controlled by limited fluvial discharge and high evaporation rates, which strongly influence its hydrodynamics and sedimentary processes (Gutiérrez-Moreno et al., 2008). San Andrés is an oceanic island within the Archipelago of San Andrés, Providencia and Santa Catalina in the Caribbean Sea. The site is an open coast characterized by a microtidal regime, consistent with the rest of the Colombian Caribbean coast, and exhibits a mean tidal range of approximately 0.25 m (Observatorio Ambiental de Cartagena, 2016). In the Islas del Rosario Archipelago (Isla Grande) and San Andrés Islands (Old Point), mangroves develop in protected open-coast environments associated with reef systems, where geomorphology is strongly influenced by the presence of coral reefs that modulate incoming wave energy (Díaz et al., 2000). Punta Soldado in Buenaventura is classified as an estuarine environment associated with a barrier island, where coastal reworking processes driven by waves and tides predominate (Eisinger Valderrama, 2023).



Map 1 Geomorphic settings of study sites **A**. Map of Colombia. **B.** Caribbean region. **C.** Pacific region

2.2 Selection of oceanographic and morphometric controls on wave attenuation rates

To identify the contribution of key controls on mangrove wave attenuation, we selected variables previously identified as critical in wave-vegetation interaction studies: incident wave height (H_s), volumetric vegetation density (V_d), mean tidal range, and the bathymetric change along the profile, measured at horizontal distances of one and three meters (e.g. Mazda et al., 2006; Quartel et al., 2007, Horstman et al., 2014; Sánchez-Núñez et al., 2020; Wei et al., 2025). Pronounced bathymetric shifts drive wave reflection, and, consequently, impact wave attenuation rates.

2.3 Determination of wave attenuation using primary data

2.3.1 Sensor deployment in Boca Grande, Bahía Portete, Punta Soldado and Old Point

At each study site, multiple pressure sensors were installed along cross-shore transects that extended between three and fourteen meters into the mangrove vegetation (Fig 1). Were installed $RBR\ solo^3$ pressure sensors at the mangrove edge and within the forest interior. All instruments were deployed for a minimum period of 48 hours, ensuring the acquisition of hydrodynamic data

under both high- and low-tide conditions and allowing for the assessment of temporal variability in wave forcing.

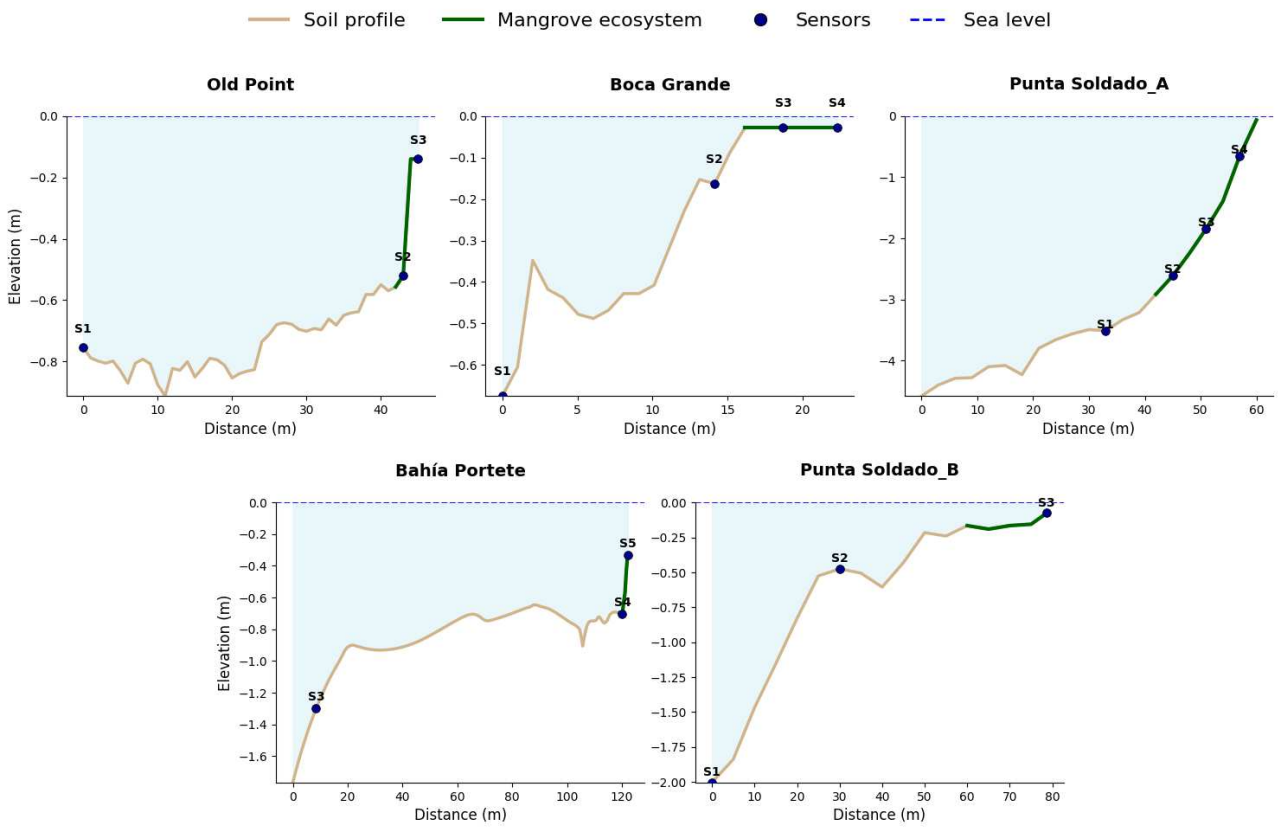


Fig 1 Bathymetric profile of the study areas. S1 (sensor 1), S2 (sensor 2), S3 (sensor 3), S4 (sensor 4) and S5 (sensor 5)

2.3.2 Morphometric characterization: bathymetric profile and volumetric density

To characterize the bathymetry governing wave propagation, including depth gradients and bottom slopes, a nearshore bed profile was surveyed using a sight level and a topographic leveling staff. Water depth measurements were collected at one-meter intervals, starting from the location of the innermost sensor and extending at least ten meters seaward along a straight transect oriented perpendicular to the shoreline. Based on the surveyed profiles, bathymetric changes within the mangrove were calculated at one and three meters from the closest seaward sensor.

Finally, volumetric density (V_d) was estimated as a dimensionless parameter representing the ratio between mangrove vegetation volume and a defined control volume within the vegetated zone, following Equation 1. To compute (V_d) measurements of root diameter and root density were

collected at 0.1 m, 0.5 m and 1.0 m above the bed, depending on site water depth. Root and stem density and diameter measurements taken at heights 0.1, 0.5 and 1.0 m represented three distinct vegetation layers above the sediment: 0.0-0.3, 0.3-0.7, and 0.7-1.3 m, respectively. The specific layers included in the V_d calculations were determined by the water depth recorded by sensors. For example, at Punta Soldado, macrotidal conditions caused a maximum inundation of 1.25 m, making vegetation structure measurements at 1.0 necessary to accurately estimate V_d. Measurements were obtained using Vernier calipers and 1 m × 1 m plots were employed to standardize sampling areas. After data collection, pressure records were downloaded from each instrument for subsequent processing.

$$V_d = \frac{\sum \pi * r_n^2 * h_n}{A_q * H_c} \quad (1)$$

Where **r** represents the radius of the root and **h** corresponds to the root height measured from the bed level, **A** represents the quadrat area and **H** corresponds to the height of the considered water volume, $\boldsymbol{A_q}$ Quadrat area, $\boldsymbol{H_c}$ Water depth considered.

2.3.3 Mangrove wave attenuation rates

Raw data obtained from the pressure sensors were processed and analyzed using the Python programming language with the Pandas library. Wave shoaling and breaking at shallow mangrove depths can obscure wave attenuation generated by vegetation (Horstman et al., 2014; Sánchez-Núñez et al., 2020). Therefore, the pressure records from the outermost sensors were used to evaluate and remove the shoaling and breaking effects through numerical simulations with the XBeach model (Roelvink et al., 2009), implemented in phase-averaged ("surfbeat") mode under stationary conditions. The model allowed reproduction of wave propagation processes over the coastal profile, including wave shoaling and breaking.

Wave attenuation rates were estimated exclusively from pressure sensors located within the mangrove forest. The outermost sensors were not included in the attenuation calculations because their primary purpose was to characterize incoming wave conditions. Subsequently, wave height values recorded by the sensors within the forest were organized to estimate wave attenuation between consecutive sensor pairs (Equation 2). This procedure enabled the estimation of

attenuation rates in areas vegetated by *R. mangle*, following approaches widely used in field-based mangrove studies (Mazda et al., 1997; Brinkman, 2006). In this way, it was possible to reproduce wave propagation and to contextualize the measured signals when waves reach the mangrove edge.

$$r = \frac{\Delta H}{\Delta x} * \frac{1}{H_{incident}} \qquad (2)$$

Where $\boldsymbol{\Delta H}$ represents the difference in wave height (H_s) between two sensors; $\boldsymbol{\Delta x}$ is the distance in meters separating the sensors and $\boldsymbol{H_{incident}}$ corresponds to the H_s at the upstream sensor of the pair.

From a physical perspective, variations in wave height along the transect are associated with changes in the energy balance (Holthuijsen, 2007). In mangrove environments, these variations are controlled by the combined action of transformation processes induced by bathymetry, bottom friction, and the hydrodynamic resistance generated by vegetation. *R. mangle* root system produces drag forces that dissipate wave momentum and can generate turbulence within the water column (Méndez & Losada, 2004; Massel et al., 1999), while bathymetric changes, depending on their magnitude and the relative depth (wave height/water depth) drive wave shoaling, breaking reflection.

2.4 Wave attenuation data

Secondary data on wave attenuation were obtained from scientific literature. Data for the Bahía Cispatá and Punta Mestizos were extracted from the study conducted by Sánchez-Núñez et al. (2020), from which values corresponding to the three analyzed sites were used. In this dataset, sites PM_1 and PM_2 (PM - Punta Mestizos) exhibit wave reflection effects associated with the presence of a geomorphological step. Wave attenuation data for the Islas del Rosario Archipelago were taken from Vanegas et al. (2019), as reported in the supplementary material of Sánchez-Núñez et al. (2020). For all sites included in the analysis, only those with available information on the morphometric and oceanographic variables of interest were considered (Table 3 in the Supplementary Material).

2.5 Data analysis

Wave attenuation rates were compared across geomorphic types, wave exposure levels, and between sites with the presence or absence of root epiphytic-bivalves, using non-parametric statistical tests. Additionally, volumetric density was compared between sites based on the occurrence of these bivalves. To estimate the influence of the five selected regulating variables on mangrove wave attenuation rates, a multivariate linear regression analysis was implemented. Variables were incorporated into the model sequentially in order to evaluate their individual and combined effects, and to assess potential relationships among them. This approach allowed the simultaneous influence of all five regulators on wave attenuation rates to be examined. In addition, simple linear regressions were performed to evaluate whether each regulating variable exerted an individual influence on wave attenuation rates. Model selection was based on Akaike's information criterion (AIC), Bayesian Information Criterion (BIC) and variable significance.

3. Results

3.1 Variability in Volumetric density and Wave Attenuation Rates across Geomorphic settings

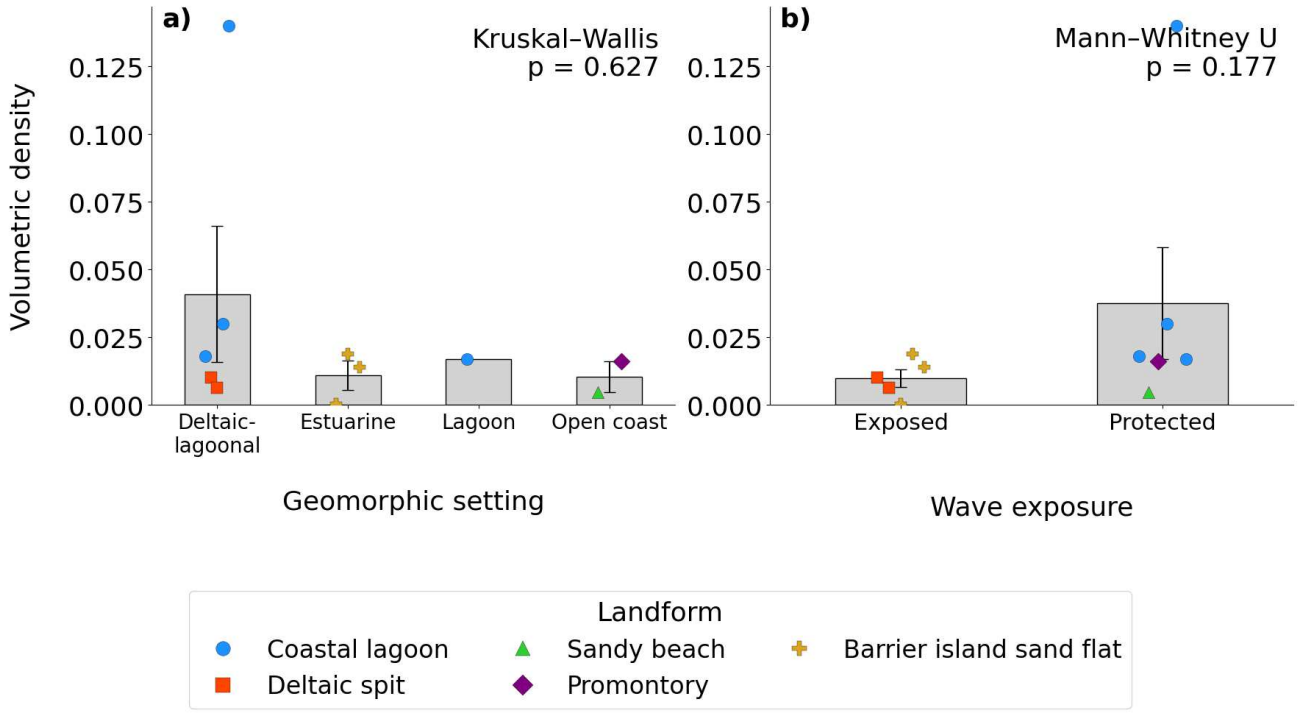


Fig 2 a) volumetric density in relation to geomorphic setting. **b)** volumetric density in relation to the forest exposure level

Boca Grande (BG) exhibited the highest mangrove volumetric density values (0.14 and 0.03), followed by Bahía Cispatá (0.018), whereas the lowest values were recorded at a site in Punta Soldado (0.0003). At the ecosystem scale, the highest wave attenuation rate was observed in BG, with a maximum value of 0.49 m^{-1}, coinciding with sectors characterized by high *R. mangle* root density. In contrast, Punta Soldado exhibited the lowest attenuation rates, with an average value of 0.05.

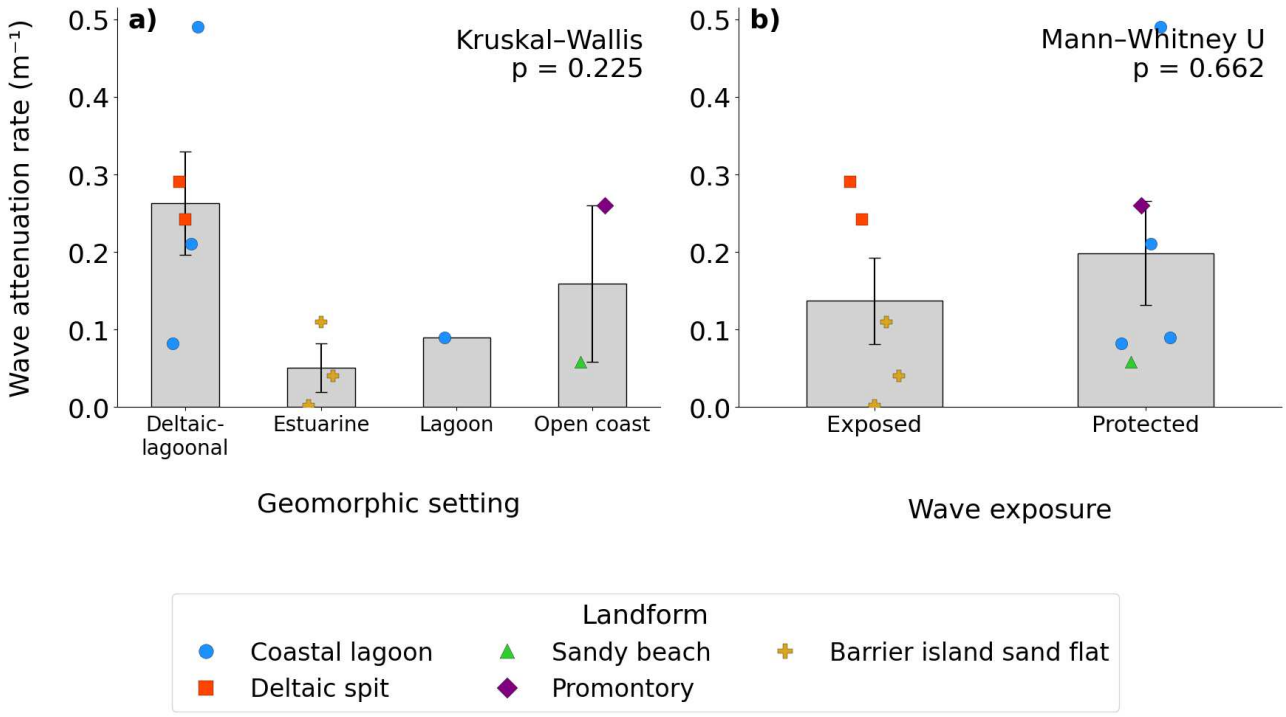


Fig 3 a) wave attenuation rate provided by the mangrove ecosystem in relation to the coastal environment. **b)** attenuation rate in relation to the forest exposure level

Volumetric density showed no differences among geomorphic settings ($p = 0.627$), alongside high within-group variability in deltaic-lagoonal systems and coastal lagoon landforms (Fig 2a). Likewise, wave attenuation rates were highly variable within deltaic-lagoonal, open coast settings, and coastal lagoon landforms. Attenuation rates were highest in deltaic-lagoonal settings and lowest at estuarine sites, but these differences were not statistically significant. Coastal lagoon

landforms where epiphytic organisms are present have significantly higher volumetric densities compared to sites lacking these organisms (p = 0.024) (Fig 4a). However, wave attenuation rates in coastal lagoon landforms where epiphytic organisms are present have higher, but not different attenuation rates compared to sites lacking these organisms (Fig 4b). On the other hand, mean volumetric density was 3.8-fold higher in protected sites compared to exposed sites, but showed no significant difference (*Mann-Whitney U*, p = 0.177) (Fig 2b). Wave attenuation rates did not differ between protected and exposed sites (Fig 3b).

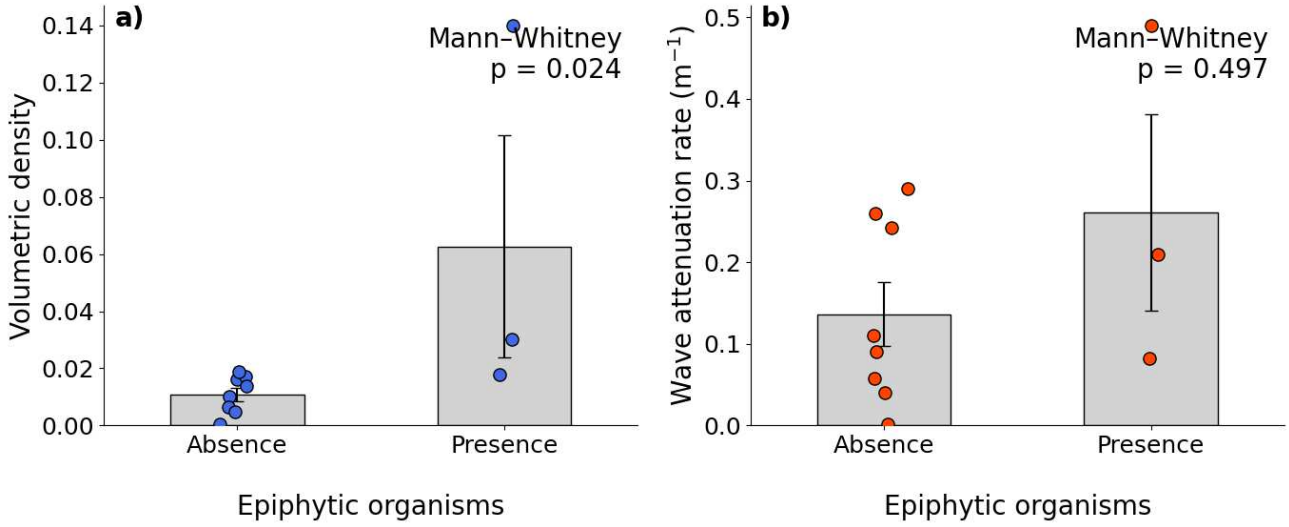


Fig 4 a) Relationship between mangrove volumetric density and the presence or absence of root-epiphytic bivalves. **b)** Wave attenuation rate according to the presence or absence of root-epiphytic bivalves

3.2 Oceanographic and morphometric drivers of wave attenuation rates

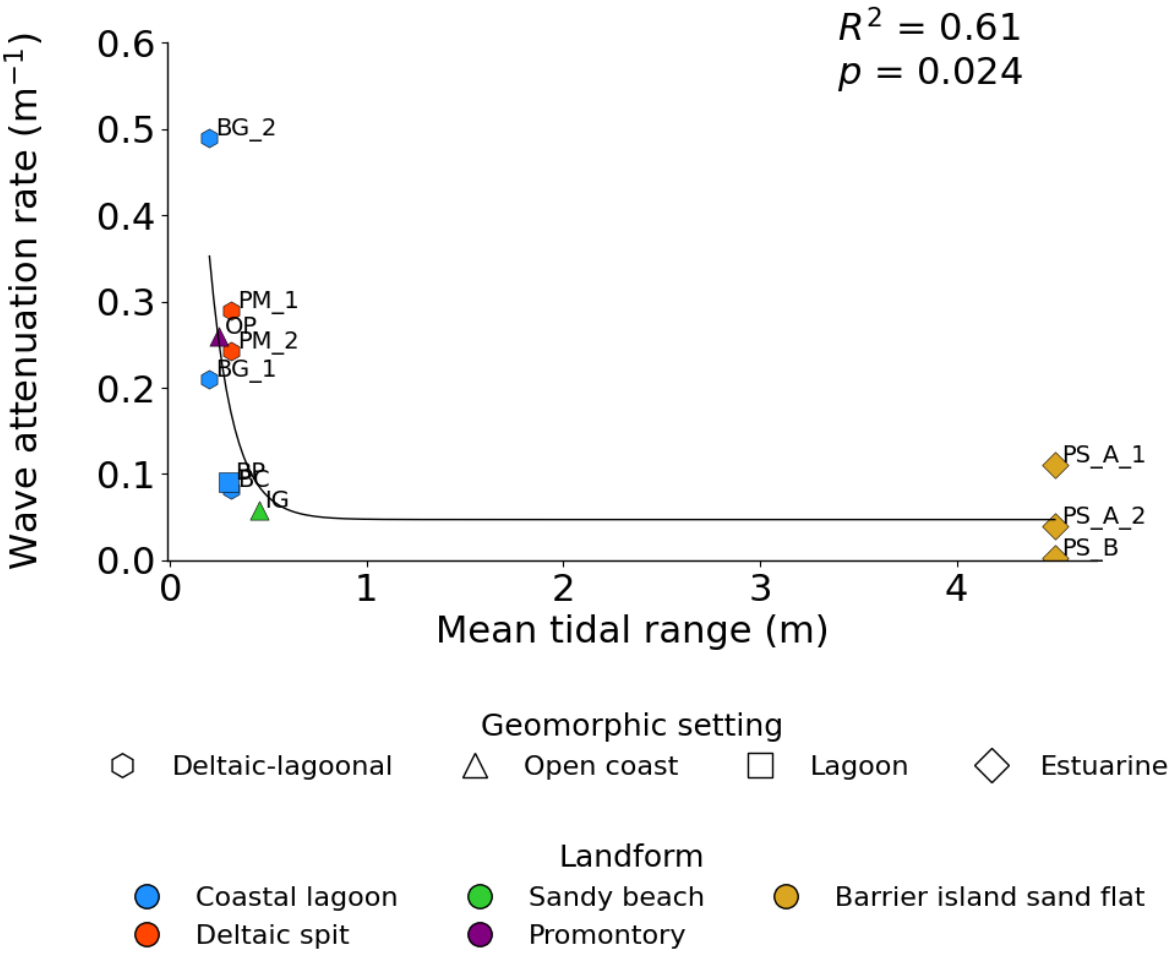


Fig 5 Relationship between mean tidal range and attenuation rate. Study sites include: BG_1 and BG_2 (Boca Grande, Ciénaga Grande de Santa Marta); BC, PM_1, and PM_2 (Bahía de Cispatá and Punta Mestizos, Sinú River Delta); OP (Old Point, San Andrés Islas); IG (Isla Grande, Archipelago Islas del Rosario); BP (Bahía Portete, La Guajira) and PS_A_1, PS_A_2 and PS_B (Punta Soldado, Buenaventura). Data points are differentiated by geomorphic setting and landform

After selecting the three best multivariate models based on their adjusted R^2, Bayesian Information Criterion and the Akaike Information Criterion (Table 2), Model II was selected as the most parsimonious model; with most of its variables statistically significant and the remaining variable close to the significance threshold. In this model, which incorporated both morphometric and oceanographic variables, yielded a *p-value* of 0.004 and an adjusted R^2 of 0.760. The morphometric regulator included (V_d) was positively associated with mangrove wave attenuation

rates (coefficient = 2.840). Among oceanographic regulators, significant wave height showed a positive trend (coefficient = 0.579) while mean tidal range was negatively related to attenuation rate (coefficient = −0.047). Fig 5 illustrates the relationship between tidal range and wave attenuation across the different geomorphic settings and landforms evaluated (*p value* = 0.024). A Pearson correlation test revealed a significant positive correlation between mean tidal range and incident wave height (r = 0.851, *p value* = 0.0009), indicating that these two variables are covary.

Table 2. Multivariate analysis results for the ecosystem-specific wave attenuation rate, with outputs including the coefficient (Coeff), standard error (Std err), t-statistic (t), Bayesian Information Criterion (BIC) and Akaike information criterion (AIC). The selected model was indicated with double asterisks (**) based on their R^2 values, adjusted R^2, *p*-value, number of significant variables, BIC and AIC.

Model	Wave attenuation driver	Regression statistics				Model fit statistics			BIC	AIC
		Coeff	Std err	t	*p - value*	*p - value* (F)	R - squared	Adjusted R - squared		
I	Volumetric density	2.794	0.613	4.558	0.006	0.012	0.909	0.818	-24.485	-26.872
	Bathymetric change at one meter	-0.283	0.190	-1.491	0.196					
	Bathymetric change at three meters	0.144	0.110	1.323	0.243					
	Mean tidal range	-0.038	0.013	-2.869	0.035					
	Incident wave height	0.241	0.242	1.739	0.142					
II**	Volumetric density	2.840	0.617	4.603	0.002	0.004	0.832	0.760	-22.526	-24.118
	Mean tidal range	-0.047	0.015	-3.256	0.014					
	Incident wave height	0.579	0.264	2.201	0.064					
III	Volumetric density	2.821	0.799	3.530	0.010	0.014	0.760	0.657	-18.568	-20.160

	Bathymetric change at one meter	-0.409	0.253	-1.620	0.149					
	Bathymetric change at three meters	0.209	0.146	1.429	0.196					

4. Discussion

4.1 Variability in Wave Attenuation Rates across Geomorphic Settings and Landforms

The present study revealed differences in mangrove wave attenuation rates between geomorphic settings, with higher rates in deltaic-lagoonal environments and lower rates in estuarine systems. However, this pattern was not statistically robust, likely due to the high variability within deltaic-lagoonal environments and the limited number of observations.

Although a difference in wave attenuation rates between deltaic-lagoonal and estuarine systems is expected owing to contrasting tidal ranges, high intra-setting variability in other wave attenuation drivers, such as volumetric density and wave height (Table 1), likely obscures any significant trend. In fact, the variability of these drivers is very high even within the same landform or site. Within single study areas, the coefficients of variation for incident wave height and root volumetric density averaged 36% and 68%, respectively. Such results suggest that local variations in wave attenuation can rival or even surpass differences across geomorphic settings.

On the other hand, tidal range is a clear driver of attenuation rates as found in this study and others (Sánchez-Núñez et al., 2020; Zhou et al. 2022); the efficiency of wave height reduction by mangroves increases under low inundation conditions, a mechanism discussed in detail in sentient 4.2. Therefore, we expect that despite high inter-setting variability on attenuation rates and drivers, a clear difference between estuarine and other geomorphic settings associated with microtidal regimes (e. g. open coast and lagoonal types) would emerge with more observations.

Volumetric density was influenced more clearly by epiphytic bivalves than by wave exposure. However, the pronounced differences in volumetric density between protected and exposed sites, together with the exclusive presence of epiphytic bivalves in protected sites, suggest that

multifactorial regulation of wave attenuation (section 4.2) likely masked significant differences. Thus, volumetric density is influenced not only by roots colonization by epibiont, but also by wave exposure conditions that favor such colonization. Root fouling communities are a well documented feature of *R. mangle* systems, where sessile organisms colonize submerged prop roots and alter root structure (Ellison and Farnsworth, 1992). In sheltered environments, Woodroffe (1992) noted that low wave energy promotes the establishment of aerial roots as well as the accumulation of organisms on prop roots. Barnacles and bivalves in particular can extensively colonize submerged roots, contributing to the system's volumetric density and increasing hydraulic friction (Dueñas-Lagos et al., 2025). In contrast, wave energetic environments, such as our exposed sites, may limit the development of dense root structure and constrain epiphytic organisms.

In this context, the lower volumetric densities observed at exposed sites may reflect greater physical disturbance and constrain the establishment of epiphytic organisms. Despite the observed differences in volumetric density (V_d), wave attenuation rates were similar between sheltered and exposed sites. These findings indicate that mangroves can maintain their wave attenuation capacity even under exposed, high-energy hydrodynamic conditions. From a theoretical perspective, higher volumetric density would be expected to increase flow resistance and, consequently, wave attenuation (Mazda et al., 1997), a relationship that has been confirmed in field studies (Horstman et al., 2014). However, results of multivariate regressions (section 4.2) suggest that volumetric density does not act in isolation, but rather depends on its interaction with other wave attenuation regulators.

Collectively, these results indicate that wave attenuation in mangrove ecosystems cannot be attributed exclusively to geomorphic settings, tidal ranges or vegetation density. Instead, attenuation emerges from coupled eco-hydrodynamic interactions operating across multiple spatial scales, where tidal regime, wave exposure and vegetation structure jointly regulate wave transformation processes (Koch et al., 2009).

4.2 Drivers and Mechanisms of Mangrove Wave Attenuation

Multivariate analysis revealed that variability in wave attenuation rates is influenced by the interaction between volumetric density and hydrodynamic forcing variables. In all models, V_d

emerged as the most consistent predictor. Although its effect is not apparent in simple comparisons, it becomes significant when analyzed in combination with other variables. Similar findings have been reported in wave flume experiments and field studies, where the complexity of the root system is directly associated with increased hydraulic friction and drag forces (Horstman et al., 2014; Zhang et al., 2015; Wei et al., 2025). Horstman et al. (2012) documented an increase in attenuation associated with higher root density, highlighting the role of submerged vegetation. Similarly, Mullarney et al. (2017) documented considerable spatial variability in vegetation induced drag within a wave-exposed mangrove forest.

In Model II, the negative relation between tidal range and wave attenuation shows that higher inundation levels reduce the mangrove's capacity to attenuate waves. This finding is consistent with the physical understanding of wave–vegetation interactions, as increased water depth limits the interaction between the flow and the densest portion of the root system near the substrate, thereby reducing drag forces (Mazda et al., 2006; Nepf, 2012). This pattern is further supported by field and experimental evidence: Vo-Luong and Massel (2008), Horstman et al. (2014) and Zhang et al. (2022) demonstrated that the efficiency of wave height reduction by mangroves increases under low inundation conditions. This is because the larger root density present close to the ground comes into contact with the wave flow, enhancing hydrodynamic resistance. This pattern is also consistent with observations made by Zhou et al. (2022) in China, where attenuation varied markedly across tidal zones depending on relative water depth. This behavior is related to the role of volumetric density, which amplifies frictional and drag forces by increasing the surface area in contact with waves (Mazda et al., 1997; Luhar et al., 2010; Zhang et al., 2012).

The association between significant wave height (H_s) and wave attenuation is complex and modulated by tidal range, as evidenced by the correlation of these variables and their joint presence in the model. Higher tides corresponded to greater wave heights due to reduced wave breaking in deeper water, consistent with tidally modulated depth-limited breaking documented in other shallow-water systems (Becker et al., 2014). Conversely, attenuation was strongest when large waves coincided with low tides and high near-substrate root density (section 4.1), so the influence of wave height was expressed mainly through its interaction with other regulators, consistent with evidence that relative wave height, the ratio of wave height to water depth, best predicts mangrove wave dissipation (Hu et al., 2025). This direct relationship stems from higher orbital velocities that

induce stronger turbulence and hydrodynamic resistance, accelerating attenuation for larger waves (Dang et al., 2026).

Bathymetric elevation change was not retained among these regulators. Local bathymetric changes are known, in principle, to shape wave transformation — altering seabed roughness, wave reflection and breaking (Massel et al., 1999; Möller, 2006; Sánchez-Núñez et al., 2020; Lopez-Arias et al., 2024) —and to modify local water depth and wave– vegetation interaction (Mazda et al., 2006; Méndez and Losada, 2004). In our dataset, however, this mechanism did not translate into a measurable contribution to attenuation showing that other regulators are more important drivers of wave attenuation.

Overall, wave attenuation by mangroves cannot be attributed to any single regulator: vegetation density defines the potential for drag generation, while tidal range and wave height determine the extent to which waves interact with the submerged root system, with local bathymetry likely playing a secondary, more localized role. This pattern agrees with recent numerical modelling evidence that relative wave height combined with submerged volumetric density best explains mangrove wave attenuation (Dang et al., 2026), indicating that attenuation emerges from coupled eco-hydrodynamic processes rather than isolated drivers.

5. Conclusions and Implications

We hypothesized that geomorphic setting would strongly influence mangrove wave attenuation, through regulators such as tidal range, and as it shapes other mangrove ecosystem services (Rovai et al., 2018; Twilley et al., 2018). Although attenuation rates varied noticeably between deltaic-lagoonal and estuarine sites, the lack of a consistent geomorphic pattern is likely due to the high variability of wave height and volumetric density across geomorphic settings and landforms that interact with tidal range to drive attenuation rates. Such interplay among wave attenuation regulators likely obscures a clearer difference between geomorphic settings. In addition, while this study integrates four geomorphic types across six study areas and eleven case studies, broader sampling is needed to better capture differences in wave attenuation across geomorphic settings, given the high internal variability within each setting.

Wave attenuation variability was demonstrated to be driven by the interaction of biophysical and hydrological regulators nested within geomorphic settings. The integrated nature and heterogeneity of such regulators implies that the wave attenuation capacity of mangroves can greatly vary within the same geomorphic setting and site.

Tidal range was consistently identified as a significant regulator of attenuation within the multivariate model. Even though its effect did not translate into a statistically robust difference among geomorphic settings. Although high internal variability and sample size limited statistical separation among, we predict that geomorphic settings characterized by narrower tidal ranges - such as open coast or microtidal deltaic-lagoonal systems - will sustain higher wave attenuation than macrotidal, estuarine-type settings. Among the interacting regulators, root volumetric density emerged as the most consistent predictor of wave attenuation rates; and the influence of epiphytic organisms colonization on prop roots underscores the importance of such root system complexity. However, the similarity in attenuation between sheltered sites with epiphytic bivalves and exposed sites corroborates that this process responds to multiple coupled physical mechanisms.

Our findings emphasize the need to integrate ecological and physical context when evaluating mangroves as Nature-Based Solutions for coastal protection. Accordingly, these results provide key insights for the design of Nature-based Solutions (NbS): the effectiveness of mangroves in coastal protection depends on multiple system factors that are variable at local and regional scales. Restoration and conservation strategies should focus, as suggested before (Sánchez-Núñez et al., 2020), on optimizing root volumetric density and favoring root-epiphytic associations. By managing these drivers, mangroves can be more effectively used as adaptive tools to enhance coastal resilience.

Finally, this study evaluated only attenuation rates per unit distance within the fringe mangrove, without considering the cumulative effect associated with the total forest width. The capacity of mangroves to provide coastal protection depends not only on attenuation efficiency per meter, but also on the spatial extent of the ecosystem. These factors should be considered when assessing which geomorphic settings provide the greatest wave attenuation.

6. Acknowledgments

This study was funded by the Colombian Government's GENERAL ROYALTY SYSTEM (SGR) through the project entitled "EVALUACIÓN DE SERVICIOS ECOSISTÉMICOS PROVISTOS POR HUMEDALES COSTEROS EN EL CARIBE COLOMBIANO / UNIVERSIDAD NACIONAL DE COLOMBIA" with project number in Minciencias: 82219, Contract: ICETEX 2023 - 0780 and the project entitled "RESEARCH ON ECOSYSTEM SERVICES DERIVED FROM MANGROVE FORESTS IN THE COLOMBIAN PACIFIC: VALLE DEL CAUCA, NARIÑO, CAUCA, CHOCÓ" with BPIN 2020000100054.

7. CrediT authorship contribution statement

Maria Fernanda Acosta Silva: Conceptualization, methodology, writing of the original draft, data processing. David Alejandro Sánchez-Núñez: Conceptualization, methodology, research, review, editing, and fundraising. César Padilla-Mendoza: methodology, data processing, research, and review. Jose Ernesto Mancera-Pineda: Conceptualization, review and fundraising.

8. Declaration of competing interest

The authors declare that they have no known competing financial interests or personal relationships that could have appeared to influence the work reported in this paper.

9. Ethical approval and consent to participate

Not applicable. This study did not involve human participants, human data, or animal subjects requiring ethical approval.

10. Consent for publication

Not applicable. This manuscript does not contain any individual person's data in any form.

11. Data availability and material:

The datasets generated and analyzed during the current study are available from the corresponding author upon reasonable request.

12. Bibliography

Alongi, D. M. (2009). The energetics of mangrove forests. *Springer*. https://doi.org/10.1007/978-1-4020-4271-3

Banco Mundial. (2024). Costas colombianas: Un análisis integral de la erosión costera. Reporte síntesis. *Banco Mundial*.

Bao, T. Q. (2011). Effect of mangrove forest structures on wave attenuation in coastal Vietnam. *Oceanología*, 53(3), 807–818. https://doi.org/10.5697/oc.53-3.807

Becker, J. M., Merrifield, M. A., & Ford, M. R. (2014). Water level effects on breaking wave setup for Pacific Island fringing reefs. *Journal of Geophysical Research: Oceans*, 119(2), 914–935. https://doi.org/10.1002/2013JC009373

Bernal, G. (1996). Caracterización geomorfológica de la llanura deltaica del río Magdalena con énfasis en el sistema lagunar de la Ciénaga Grande de Santa Marta, Colombia. *Boletín de Investigaciones Marinas y Costeras*, 25, 19–48.

Beudin, A., Kalra, T. S., Ganju, N. K., & Warner, J. C. (2017). Development of a coupled wave–flow–vegetation interaction model. *Computers & Geosciences*, 100, 76–86. https://doi.org/10.1016/j.cageo.2016.12.010

Blanco-Libreros, J. F., López-Rodríguez, S. R., Valencia-Palacios, A. M., Pérez-Vega, G. F., & Álvarez-León, R. (2022). Mangroves from rainy to desert climates: Baseline data to assess future changes and drivers in Colombia. *Frontiers in Forests and Global Change*, 5, 772271. https://doi.org/10.3389/ffgc.2022.772271

Brinkman, R. M. (2006). Wave attenuation in mangrove forests: An investigation through field and theoretical studies.

Bustos-Montes, D., Santafé-Muñoz, A., Grijalba-Bendeck, M., Jáuregui, A., Franco-Herrera, A., & Sanjuan-Muñoz, A. (2012). Bioecología de la lisa (Mugil incilis Hancock) en la bahía de Cispatá, Caribe colombiano. *Boletín de Investigaciones Marinas y Costeras*, 41(2), 447–461.

Cendales, M. H., Zea, S., & Díaz, J. M. (2002). Geomorfología y unidades ecológicas del complejo de arrecifes de las Islas del Rosario e Isla Barú (Mar Caribe, Colombia). *Revista de la Academia Colombiana de Ciencias Exactas, Físicas y Naturales*, 26(101), 497–510.

Dang, H. V., Tomiczek, T., Shin, S., Cox, D. T., & Lomonaco, P. (2026). OpenFOAM-based numerical modeling on wave transformation and attenuation in idealized prototype-scale mangrove forest: Regular and random waves. *Ocean Engineering*, 359.

Díaz, J. M., Barrios, L. M., Cendales, M. H., Garzón-Ferreira, J., Geister, J., López-Victoria, M., Ospina, G. H., Parra-Velandia, F., Pinzón, J. H., Vargas-Ángel, B., Zapata, F. A., & Zea, S. (2000). Áreas coralinas de Colombia (Serie de Publicaciones Especiales No. 5). Instituto de Investigaciones Marinas y Costeras "José Benito Vives de Andréis" (INVEMAR).

Dueñas-Lagos, A., Mancera-Pineda, J. E., Campos-Campos, H., & Dueñas-Ramírez, P. (2025). Faunal assemblages associated with submerged *Rhizophora mangle* roots in the Colombian Caribbean. *Bulletin of Marine Science*, 101(3), 1083–1098.

Echeverry Hernández, J. P., Mancera-Pineda, J. E., Sánchez-Núñez, D. A. (2025). Migration of deltaic and open water mangrove forests in response to environmental factors. *Frontiers in Marine Science*, 12, 1569857.

Ellison, A. M., & Farnsworth, E. J. (1992). The ecology of Belizean mangrove-root fouling communities: Patterns of epibiont distribution and abundance, and effects on root growth. *Hydrobiologia*, 247, 87–98. https://doi.org/10.1007/BF00008207

Eisinger Valderrama, K. (2023). Análisis del cambio morfológico en la línea de costa de la bahía de Buenaventura (Pacífico colombiano) a través de sensores remotos de 2016 a 2021 [Trabajo de grado, Universidad de Antioquia].

Gamboa, L., Posada, B., González, O., & Andrade-Amaya, C. (2012). Descripción física del archipiélago de San Andrés, Providencia y Santa Catalina. En DIEM (Ed.), Atlas de la reserva de la biosfera Seaflower: Archipiélago de San Andrés, Providencia y Santa Catalina (pp. 23–31). Instituto de Investigaciones Marinas y Costeras "José Benito Vives de Andréis" (INVEMAR).

Geister, J. (1973). Pleistozäne und rezente Mollusken von San Andrés (Karibisches Meer, Kolumbien) mit Bemerkungen zur geologischen Entwicklung der Insel. Mitteilungen del Instituto Colombo-Alemán de Investigaciones Científicas Punta de Betín, 7, 229–251.

Gutiérrez-Moreno, C., Alonso, D., & Segura, C. (2008). Marine protected area design for Bahía Portete–La Guajira, Colombian Caribbean. *Boletín de Investigaciones Marinas y Costeras*, 37(2), 189–212. https://doi.org/10.25268/bimc.invemar.2008.37.2.197

Holthuijsen, L. H. (2007). Waves in oceanic and coastal waters. *Cambridge University Press*.

Horstman, E. M., Dohmen-Janssen, C. M., Narra, P. M. F., van den Berg, N. J. F., & Hulscher, S. J. M. H. (2012). Wave attenuation in mangrove forests: Field data obtained in Trang, Thailand. *Coastal Engineering Proceedings*, 33, Article 38.

Horstman, E. M., Dohmen-Janssen, C. M., Narra, P. M. F., van den Berg, N. J. F., Siemerink, M., & Hulscher, S. J. M. H. (2014). Wave attenuation in mangroves: A quantitative approach to field observations. *Coastal Engineering*, 94, 47–62. https://doi.org/10.1016/j.coastaleng.2014.08.005

Hu, Z., Temmerman, S., Zhu, Q., Wang, X., Wu, J., Xu, T., Schoutens, K., Suzuki, T., Yang, Z., & Bouma, T. J. (2025). Predicting nature-based coastal protection by mangroves under extreme waves. *Proceedings of the National Academy of Sciences*, 122(12), e2410883122. https://doi.org/10.1073/pnas.2410883122

Huang, K., Hu, Z., Liu, Z., Paul, M., Xu, T., & Suzuki, T. (2024). Pinpointing the role of wave period in vegetation-induced wave attenuation. *Coastal Engineering*, 193, 104568. https://doi.org/10.1016/j.coastaleng.2024.104568

Instituto de Investigaciones Marinas y Costeras José Benito Vives de Andréis (INVEMAR). (2022). Informe del estado de los ambientes y recursos marinos y costeros en Colombia. INVEMAR.

Kjerfve, B. (1994). Coastal lagoons. En B. Kjerfve (Ed.), *Coastal lagoon processes* (pp. 1–8). Elsevier. https://doi.org/10.1016/S0422-9894(08)70006-0

Koch, E. W., Barbier, E. B., Silliman, B. R., Reed, D. J., Perillo, G. M. E., Hacker, S. D., Granek, E. F., ... (2009). Non-linearity in ecosystem services: Temporal and spatial variability in coastal protection. *Frontiers in Ecology and the Environment*, 7(1), 29–37. https://doi.org/10.1890/080126

Lopez-Arias, F., Maza, M., Calleja, F., Govaere, G., & Lara, J. L. (2024). Integrated drag coefficient formula for estimating the wave attenuation capacity of Rhizophora sp. mangrove forests. *Frontiers in Marine Science*, 11. https://doi.org/10.3389/fmars.2024.1383368

Luhar, M., Coutu, S., Infantes, E., Fox, S., & Nepf, H. (2010). Wave-induced velocities inside a model seagrass bed. *Journal of Geophysical Research: Oceans*, 115, C12005. https://doi.org/10.1029/2010JC006345

Martínez, J. O., González, J. L., Pilkey, O. H., & Neal, W. J. (2000). Barrier island evolution on the subsiding central Pacific coast, Colombia. *Journal of Coastal Research*, 16(3), 663–674.

Massel, S. R., Furukawa, K., & Brinkman, R. M. (1999). Surface wave propagation in mangrove forests. *Fluid Dynamics Research*, 24(4), 219–249. https://doi.org/10.1016/S0169-5983(98)00024-0

Mazda, Y., Magi, M., Ikeda, Y., Kurokawa, T., & Asano, T. (2006). Wave reduction in a mangrove forest dominated by Sonneratia sp. *Wetlands Ecology and Management*, 14, 365–378. https://doi.org/10.1007/s11273-005-5388-0

Mazda, Y., Wolanski, E., King, B., Sase, A., Ohtsuka, D., & Magi, M. (1997). Drag force due to vegetation in mangrove swamps. *Mangroves and Salt Marshes*, 1, 193–199.

Méndez, F. J., & Losada, I. J. (2004). An empirical model to estimate the propagation of random breaking and nonbreaking waves over vegetation fields. *Coastal Engineering*, 51(2), 103–118. https://doi.org/10.1016/j.coastaleng.2003.11.003

Möller, I. (2006). Quantifying saltmarsh vegetation and its effect on wave height dissipation: Results from a UK east coast saltmarsh. *Estuarine, Coastal and Shelf Science*, 69(3–4), 337–351. https://doi.org/10.1016/j.ecss.2006.05.003

Mullarney, J. C., Henderson, S. M., Reyns, J. A. H., Norris, B. K., & Bryan, K. R. (2017). Spatially varying drag within a wave-exposed mangrove forest and on the adjacent tidal flat. *Continental Shelf Research*, 147, 102–113. https://doi.org/10.1016/j.csr.2017.06.019

Narayan, S., Beck, M. W., Reguero, B. G., Losada, I. J., van Wesenbeeck, B., Pontee, N., ... & Burks-Copes, K. A. (2016). The effectiveness, costs and coastal protection benefits of natural and nature-based defences. *PLoS ONE*, 11(5), e0154735. https://doi.org/10.1371/journal.pone.0154735

Nepf, H. M. (2012). Flow and transport in regions with aquatic vegetation. *Annual Review of Fluid Mechanics*, 44, 123–142. https://doi.org/10.1146/annurev-fluid-120710-101048

Niño, D. C., & Eisinger, K. A. (2025). Assessment of coastal erosion and accretion in outer Buenaventura Bay between 1969 and 2023. *CIOH Scientific Bulletin*, 44(1), 29–39. https://doi.org/10.26640/22159045.2025.646

Observatorio Ambiental de Cartagena. (2016). Pleamares en la costa Caribe colombiana: Análisis y perspectivas. *EPA Cartagena*.

Ruiz-Ochoa, M. A. R., Bernal, G., & Polanía, J. (2008). Influencia del río Sinú y el mar Caribe en el sistema lagunar de Cispatá. *Boletín de Investigaciones Marinas y Costeras*, 37(1), 31–51. https://doi.org/10.25268/bimc.invemar.2008.37.1.180

Perdomo-Trujillo, L. V., Mancera-Pineda, J. E., Medina-Calderón, J. H., Sánchez-Núñez, D. A., & Schnetter, M. L. (2021). Effect of restoration actions on organic carbon pools in the lagoon–delta Ciénaga Grande de Santa Marta, Colombian Caribbean. *Water*, 13(9), 1297. https://doi.org/10.3390/w13091297

Piccardi, M., Correa, I., & Pranzini, E. (2020). Cispatá Bay and Mestizos evolution as reconstructed from old documents and maps (16th–20th century). *Journal of Marine Science and Engineering*, 8(9), 669. https://doi.org/10.3390/jmse8090669

Quartel, S., Kroon, A., Augustinus, P. G. E. F., van Santen, P., & Tri, N. H. (2007). Wave attenuation in coastal mangroves in the Red River Delta, Vietnam. *Journal of Asian Earth Sciences*, 29(4), 576–584. https://doi.org/10.1016/j.jseaes.2006.05.008

Rodríguez-Rodríguez, J. A., Pineda, J. M., Trujillo, L. P., Rueda, M., & Ibarra-Gutiérrez, K. P. (2018). Ciénaga Grande de Santa Marta: The largest lagoon-delta ecosystem in the Colombian Caribbean. En The Wetland Book (pp. 1–16). *Springer*.

Roelvink, D., Reniers, A., van Dongeren, A., van Thiel de Vries, J., McCall, R., & Lescinski, J. (2009). Modelling storm impacts on beaches, dunes and barrier islands. *Coastal Engineering*, 56(11–12), 1133–1152. https://doi.org/10.1016/j.coastaleng.2009.08.006

Rovai, A. S., Twilley, R. R., Castañeda-Moya, E., Riul, P., Cifuentes-Jara, M., Manrow-Villalobos, M., Horta, P. A., Simonassi, J. C., Fonseca, A. L., & Pagliosa, P. R. (2018). Global controls on carbon storage in mangrove soils. *Nature Climate Change*, 8, 534–538. https://doi.org/10.1038/s41558-018-0162-5

Samiksha, S. V., Vethamony, P., Bhaskaran, P. K., Pednekar, P., Jishad, M., & James, R. A. (2019). Attenuation of wave energy due to mangrove vegetation off Mumbai, India. *Energies*, 12(22), 4286. https://doi.org/10.3390/en12224286

Sánchez-Núñez, D. A., Bernal, G., & Mancera-Pineda, J. E. (2019). The relative role of mangroves on wave erosion mitigation and sediment properties. *Estuaries and Coasts*, 42, 2124–2138. https://doi.org/10.1007/s12237-019-00628-9

Sánchez-Núñez, D. A., Mancera-Pineda, J. E., & Osorio, A. F. (2020). From local- to global-scale control factors of wave attenuation in mangrove environments and the role of indirect mangrove wave attenuation. *Estuarine, Coastal and Shelf Science*, 245, 106926. https://doi.org/10.1016/j.ecss.2020.106926

Simpson, M. C., Scott, D., Harrison, M., Sim, R., Silver, N., O'Keeffe, E., Harrison, S., Taylor, M., Lizcano, G., Rutty, M., Stager, H., Oldham, J., Wilson, M., New, M., Clarke, J., Day, O. J., Fields, N., Georges, J., Waithe, R., & McSharry, P. (2010). Quantification and magnitude of losses and damages resulting from the impacts of climate change: Modelling the transformational impacts and costs of sea level rise in the Caribbean. *United Nations Development Programme.*

Twilley, R. R., Rovai, A. S., & Riul, P. (2018). Coastal morphology explains global blue carbon distributions. *Frontiers in Ecology and the Environment*, 16(9), 503–508. https://doi.org/10.1002/fee.1937

Vanegas, C., Osorio, A. F., & Urrego, L. E. (2019). Wave dissipation across a Rhizophora mangrove patch on a Colombian Caribbean island: An experimental approach. *Ecological Engineering*, 130, 64–75.

van Zelst, V. T., Dijkstra, J. T., van Wesenbeeck, B. K., Eilander, D., Morris, E. P., Winsemius, H. C., de Vries, M. B., et al. (2021). Cutting the costs of coastal protection by integrating vegetation in flood defences. *Nature Communications*, 12, 6533. https://doi.org/10.1038/s41467-021-26887-4

Vo-Luong, P., & Massel, S. R. (2008). Energy dissipation in non-uniform mangrove forests of arbitrary depth. *Journal of Marine Systems*, 74(1–2), 603–622. https://doi.org/10.1016/j.jmarsys.2008.05.004

Wei, X., Mo, W., Xiong, L., Hu, X., & Cheng, H. (2025). Field investigation of wave attenuation in a mangrove forest dominated by Avicennia marina (Forsk.) Vierh. *Plants*, 14(1), 135. https://doi.org/10.3390/plants14010135

Woodroffe, C. D. (1992). Mangrove sediments and geomorphology. En A. I. Robertson & D. M. Alongi (Eds.), Tropical mangrove ecosystems (pp. 7–41). *American Geophysical Union*.

Worthington, T. A., zu Ermgassen, P. S. E., Friess, D. A., et al. (2020). A global biophysical typology of mangroves and its relevance for ecosystem structure and deforestation. *Scientific Reports*, 10, 14652. https://doi.org/10.1038/s41598-020-71194-5

Zhang, K., Liu, H., Li, Y., Xu, H., Shen, J., Rhome, J., & Smith, T. J. (2012). The role of mangroves in attenuating storm surges. *Estuarine, Coastal and Shelf Science*, 102–103, 11–23. https://doi.org/10.1016/j.ecss.2012.02.021

651 Zhang, X., Chua, V. P., & Cheong, H. F. (2015). Hydrodynamics in mangrove prop roots and their
652 physical properties. *Journal of Hydro-Environment Research*, 9(2), 281–294.
653 https://doi.org/10.1016/j.jher.2014.07.010
654 Zhang, X., Lin, P., & Chen, X. (2023). Experimental investigation of wave attenuation by
655 mangrove forests with submerged canopies. *Coastal Engineering*, 188, 104403.
656 https://doi.org/10.1016/j.coastaleng.2023.104403
657 Zhang, X., Lin, P., & Chen, X. (2022). Coastal protection by planted mangrove forest during
658 Typhoon Mangkhut. *Journal of Marine Science and Engineering*, 10(9), 1288.
659 https://doi.org/10.3390/jmse10091288
660 Zhou, X., Dai, Z., Pang, W., Wang, J., & Long, C. (2022). Wave attenuation over mangroves in
661 the Nanliu Delta, China. *Frontiers in Marine Science*, 9, 874818.
662 https://doi.org/10.3389/fmars.2022.874818
663

Figure captions

Map 1 Geomorphic settings of study sites **A**. Map of Colombia. **B.** Caribbean region. **C.** Pacific region

Fig 1 Bathymetric profile of the study areas. S1 (sensor 1), S2 (sensor 2), S3 (sensor 3), S4 (sensor 4) and S5 (sensor 5)

Fig 2 a) volumetric density in relation to geomorphic setting. **b)** volumetric density in relation to the forest exposure level

Fig 3 a) wave attenuation rate provided by the mangrove ecosystem in relation to the coastal environment. **b)** attenuation rate in relation to the forest exposure level

Fig 4 a) Relationship between mangrove volumetric density and the presence or absence of root-epiphytic bivalves. **b)** Wave attenuation rate according to the presence or absence of root-epiphytic bivalves

Fig 5 Relationship between mean tidal range and attenuation rate. Study sites include: BG_1 and BG_2 (Boca Grande, Ciénaga Grande de Santa Marta); BC, PM_1, and PM_2 (Bahía de Cispatá and Punta Mestizos, Sinú River Delta); OP (Old Point, San Andrés Islas); IG (Isla Grande, Archipelago Islas del Rosario); BP (Bahía Portete, La Guajira) and PS_A_1, PS_A_2 and PS_B (Punta Soldado, Buenaventura). Data points are differentiated by geomorphic setting and landform

Material complementary

Table 3. H_s: significant wave height, TR: tidal range, V_d volumetric density, r: wave attenuation rate, R: presence of wave reflection at mangrove edge, BC1: bathymetric change at one meter scale, BC3: bathymetric change at three meter scale, REB: root-epiphytic bivalve presence

Locality	**Acronyms**	r	H_s	TR	V_d	R	$BC1$	$BC3$	REB	**Species**
Bahía de Cispatá	BC	0.08	0.04	0.31	0.0179	0	0.05	0.34	1	*R. mangle*
Punta Mestizos	PM_1	0.29	0.25	0.31	0.0101	1	0.10	0.48	0	*R. mangle*
Punta Mestizos	PM_2	0.24	0.22	0.31	0.0063	1	0.01	0.72	0	*R. mangle*
Isla Grande	IG	0.06	0.08	0.45	0.0047	0	0.35	0.30	0	*R. mangle*
Old Point Mangrove Regional Park	OP	0.26	0.02	0.25	0.0160	0	0.01	0.43	0	*R. mangle*
Boca Grande	BG_1	0.21	0.03	0.20	0.0300	0	0.01	0.13	1	*R. mangle*
Boca Grande	BG_2	0.49	0.03	0.20	0.1400	0	0.01	0.13	1	*R. mangle*
Bahía Portete	BP	0.09	0.03	0.30	0.0170	0	0.24	0.27	0	*R. mangle*
Punta Soldado	PS_B	0.00	0.28	4.50	0.0003	0	0.08	0.08	0	*R. mangle*
Punta Soldado	PS_A_1	0.11	0.30	4.50	0.0188	0	0.16	0.37	0	*R. mangle*
Punta Soldado	PS_A_2	0.04	0.13	4.50	0.0138	0	0.19	0.59	0	*R. mangle*